RSC Advances

ROYAL SOCIETY OF CHEMISTRY

www.rsc.org/advances

Synthesis, photoluminescence and Judd-Ofelt analysis of a red phosphors $LiGd_5P_2O_{13}$: Eu^{3+} for white LED

Xinguo Zhang [a,b,c] *, Liya Zhou [b], Qi Pang [b], Menglian Gong [c]

[a] College of Materials and Energy, South China Agricultural University, Guangzhou 510642, China

[b] School of Chemistry and Chemical Engineering, Guangxi University, Nanning 530004, China

[c] State Key Laboratory of Optoelectronic Materials and Technologies, School of Chemistry and Chemical Engineering, Sun Yat-Sen University, Guangzhou 510275, China

Abstract

A series of $LiGd_5P_2O_{13}$: Eu^{3+} phosphors with a red-emitting band centered at 622 nm were synthesized by high temperature solid-state reaction method. Structure-luminescence correlation, concentration quenching and thermal stability of $LiGd_5P_2O_{13}$: Eu^{3+} phosphors were studied combined with XRD, PL/PLE spectra as well as temperature-dependent PL and decay curves. The optimum concentration of Eu^{3+} doped in the $LiGd_5P_2O_{13}$ is 20 mol%, and the corresponding concentration quenching mechanism is found to be dipole/quadrupole-quadrupole interactions. Intensity parameters (Ω_2 and Ω_4) and various radiative properties such as transition rates (A), branching ratios (β) and stimulated emission cross-section (δ_e) were calculated using the Judd-Ofelt theory. $LiGd_5P_2O_{13}$: Eu^{3+} exhibited good thermal stability and its emission intensity decreased slightly at temperature above 150 °C. The CIE coordinates of $LiGd_5P_2O_{13}$: $0.20Eu^{3+}$ (0.644, 0.339) are very close to s-RGB standard red (0.640, 0.330), and the corresponding quantum efficiency is 46.5 %. The results show that LGPO: Eu^{3+} may be considered as potential red emitting phosphor for NUV/blue pumped WLEDs.

1. Introduction

Recently, white light-emitting diodes (WLEDs), which are regarded as the next-generation solid-state lighting source, have attracted more and more attention due to their outstanding merits in many aspects such as long operational lifetime, high brightness, low energy consumption and environment friendliness [1]. Currently, the commercially available WLEDs are based on a blue chip with yellow phosphor (YAG:Ce). However, this combination does not contain a red component, which leads to a low color rendering index [2]. One alternative approach to obtain white light is using near-UV (NUV) InGaN-based LED chip coated with blue/green/red tricolor phosphors [3,4]. However, the efficiency and thermal stability of currently used red phosphor is relative low compared to the other two components. Thus, there is an urgent need to develop efficient and stable red phosphors that have an excitation wavelength matching the emission wavelength of the NUV LEDs (λ_{em} = ~395 nm) and blue LEDs (λ_{em} = ~460 nm).

* Corresponding author. ***E-mail address*:** mpcc1@qq.com

Eu^{3+} is an important rare earth ion in synthesizing phosphors with excellent properties, for example Y_2O_2S: Eu^{3+} is used as a red phosphor in fluorescent lamp. Recently, many novel Eu^{3+}-doped compounds have been reported as promising candidates as potential red-emitting phosphors for LED application [5,6]. It is well-known that phosphates possess many excellent properties as phosphor hosts, i.e. low sintering temperature, the large band gap and moderate phonon energy, the high thermal and chemical stability [7]. Some Eu^{3+} doped phosphate phosphors are reported to have fairly good luminescence properties, such as $Ba_{10}F_2(PO_4)_6$: Eu^{3+} [8], $Ca_9R(PO_4)_7$: Eu^{3+} (R = Al, Lu) [9] and $Ca_{19}Mg_2(PO_4)_{14}$: Eu^{3+} [10].

The host $LiGd_5P_2O_{13}$ (abbreviated as LGPO) was firstly discovered by Chen's group in 2007 [11]. $LiGd_5P_2O_{13}$ presents a new structural type and is built up from $[Gd_5P_2O_{13}]^-$ layers and one-dimensional Li chains with an unusual Li-Li distance. However, up to now, there is no report on the red phosphors based on LGPO host by doping Eu^{3+} ions.

In this paper, a systematic investigation on photo-luminescence spectra, concentration quenching, as well as thermal quenching of LGPO: Eu^{3+} phosphor were carried out. Judd-Ofelt theory was applied to calculate the intensity parameters (Ω_2 and Ω_4) and various other radiative properties such as radiative transition rates, branching and asymmetry ratios, stimulated emission cross-section, which might provide a significant insight into the structure-luminescence correlation in LGPO: Eu^{3+} system. It is found that LGPO: Eu^{3+} is an efficient red phosphor with a high red color purity and good thermal stability. The results show that LGPO: Eu^{3+} may be considered as potential red emitting phosphor for NUV/blue pumped WLEDs.

2. Experimental

Li_2CO_3 (AR), Gd_2O_3 (AR), $NH_4H_2PO_4$ (AR) and Eu_2O_3 (4N) were used as starting materials to synthesize $LiGd_{5(1-x)}P_2O_{13}$: xEu^{3+} ($0.1 \leq x \leq 1.0$) phosphors by solid state reaction. The initial materials were weighed according to the stoichiometric ratio, and mixed in an agate mortar in ethanol media with intermittent grinding and drying. The homogeneous mixture was preheated at 300°C for 4 h, then calcined at 1150 °C for 12 h with a heating rate of 300 °C/h.

Crystalline phases of samples were identified by an X-ray diffraction (XRD, Model Rigaku-D/Max-2200PC, Japan) using Cu Kα radiation with a step size of 0.02° and a speed of 10°/min within the range from 10° to 75°. The photoluminescence excitation (PLE)/ emission (PL) spectra and luminescence decay curves of samples were measured on a Edinburgh FLS-920 Time Resolved and Steady State Fluorescence Spectrometer with a 450 W xenon lamp as an excitation light source. The internal quantum efficiency was also obtained from FLS-920 spectrometer with integrated sphere. The CIE coordinates are calculated by a software, which was developed by M.H. Chan, Department of Physics, Hong Kong Baptist University (HKBU). All the measurements were recorded at room temperature.

3. Results and discussions

3.1 XRD and structure

Fig.1a illustrates the X-ray diffraction (XRD) patterns of LGPO: xEu^{3+} (x = 0.2, 0.4, 0.6 and 0.8) phosphors with different doping Eu^{3+} contents (x). All the observed diffraction peaks can be indexed to the standard data of $LiGd_5P_2O_{13}$ reported by Chen's group [11]. No obvious impurity phase was detected when Eu^{3+} ions were doped into the host lattice, indicating that all samples are of single phase.

The structure of $LiGd_5P_2O_{13}$ belongs to the centrosymmetric space group $C2/m$ with unit cell parameters a = 18.645 Å, b = 5.625 Å, c = 12.014 Å, β = 117.55°, V = 1117.3 Å^3, and Z = 4. As shown in Fig.1b, the three-dimensional (3D) framework of $LiGd_5P_2O_{13}$ consists of isolated PO4 tetrahedra linked with Gd atoms distributed among them, and Li atoms are located in the infinite tunnels along the b-axis which are delimited by PO_4 tetrahedra and Gd polyhedra. There are five Gd polyhedra in LGPO host, i.e. Gd(1) and Gd(5) are six-coordinated, and Gd(2), Gd(3), Gd(4) are seven-coordinate. All Gd-O distances vary in the range from 2.206 to 2.605 Å, and all Gd sites possess the point symmetry of C_1. Due to the similarity of charge and ionic radius (Gd^{3+} (r = 0.94 Å) and Eu^{3+} (r = 0.95 Å) [12]), it is reasonable to purpose the substitution of Gd^{3+} by Eu^{3+}. Since Eu^{3+} ions occupy highly asymmetric sites, a red emission ($^5D_0$-$^7F_2$) whose intensity is much stronger than that of orange emission ($^5D_0$-$^7F_1$) is expected in LGPO: xEu^{3+} phosphors.

3.2 PLE and PL spectra

The PLE and PL spectra of LGPO: 0.2Eu^{3+} are shown in Fig.2a. The PLE spectrum contains a series of narrow bands locating in the range of 240-480 nm. These narrow bands could be attributed to the typical 4*f*-4*f* transition absorption bands of Eu^{3+}, in which the two intense bands centered at 395 nm and 467 nm are attributed to $^7F_0$-$^5L_6$ and $^7F_0$-$^5D_2$ transition. This demonstrates that the phosphor can be excited efficiently by near-ultraviolet and blue light. The other excitation peaks centered at 319 nm, 362 nm, 376 nm, 383 nm, 398 nm, and 415 nm correspond to the transitions from $^7F_0$ to $^5H_6$, $^5D_4$, $^5G_3$, $^5L_7$, $^5L_6$, and $^5D_3$ levels, respectively.

As shown in Fig.2a, the PL spectra are composed of four bands centered at 579, 593, 622, 652, and 706 nm assigned to the $^5D_0$-^7F_J (J = 0, 1, 2, 3, and 4) transitions of Eu^{3+}, respectively. It is known that $^5D_0$-$^7F_0$ transition is forbidden and sensitive to the crystal field, which exists only when Eu^{3+} occupies sites with local symmetries of C_n, C_{nv} or C_s [13]. The $^5D_0$-$^7F_1$ transition peak originates from magnetic dipole transition. In contrast, the radiative transitions from $^5D_0$ to $^7F_2$ and $^7F_4$ levels were electric dipole in character. The $^5D_0$-$^7F_3$ transition was forbidden from both electric and magnetic dipole considerations [14]. The $^5D_0$-^7F_J emission of the Eu^{3+} ion has a close relationship with its occupied chemical environment. When the Eu^{3+} ion was located at site with inversion symmetry, the magnetic dipole ($^5D_0$-$^7F_1$) emission transition was dominant, whereas at site without inversion symmetry, the electric dipole ($^5D_0$-$^7F_2$) transition becomes dominant [15]. Thus, the intensity ratio of $^5D_0$-$^7F_2$ to $^5D_0$-$^7F_1$, $R = I_2/I_1$, is a good way to detect the symmetry of the coordinated environment around Eu^{3+} ion. A low symmetry leads to a high value of R (>1), the opposite will lead to a low value ($1 > R > 0$). The intensity of I_2 and I_1 are defined as the area under their corresponding emission spectrum curves calculated by integrating from 606 to 640 nm and 585 to 600 nm, respectively. The asymmetry ratio R of representative sample LGPO:

$0.2Eu^{3+}$ is 7.236, which indicates that Eu^{3+} occupies the sites with no inversion symmetry, and agrees well with the result of the above structural discussion.

The CIE coordinates of $LiGd_5P_2O_{13}$: $0.2Eu^{3+}$ phosphors are calculated to be $x = 0.644$, $y = 0.339$, as shown in Fig.2b. The CIE coordinate of $LiGd_5P_2O_{13}$: $0.2Eu^{3+}$ is very close to the CIE coordinate of s-RGB standard red ($x = 0.64$, $y = 0.33$), and is considered to be better than that of the commercial Y_2O_2S: Eu^{3+} ($x = 0.622$, $y = 0.351$).

3.3 Concentration quenching

Fig.3 shows the concentration dependence of PL spectra of LGPO: xEu^{3+} samples (x = 0.1-1.0) under 395 nm excitation. LGPO: xEu^{3+} samples have the same spectral profile with the different Eu^{3+}concentration. However, the luminescence intensity increases with the doping concentrations up to 0.2. With further increase of Eu^{3+} concentration, the emission intensity decreases. The distance between the Eu^{3+} ions becomes small as the concentrations of Eu^{3+} increases; thus the probability of energy migration increases. The concentration quenching phenomena will not occur if the average distance between identical Eu^{3+} ions is so large that the energy migration is hampered;

Generally speaking, the energy transfer process usually originates from exchange interaction, radiation re-absorption or multipole-multipole interaction. To investigate the concentration quenching phenomena of the phosphor, the critical distance (R_c) between Eu^{3+} ions for energy transfer can be calculated using the relation proposed by Blasse and Grabmaier as follows [16]:

$$R_c = 2\left(\frac{3V}{4\pi x_c N}\right)^{1/3} \quad (1)$$

where V is the volume of the unit cell, x_c is the critical concentration of the activator ion, and N is the number of formula unit per unit cell. In the case of $LiGd_{5(1-x)}P_2O_{13}$: xEu^{3+} phosphors, $x_c = 0.20$, $V = 1117.30$ Å^3, and $N = 4$. Therefore, R_c was calculated to be 13.86 Å. Since the corresponding critical distance for exchange interaction is about 5~8 Å, and there is tiny overlap between PL and PLE spectrum in present case, it is deduced that the electric multipolar interaction is involved in energy transfer.

To further validate the concentration quenching effect of Eu^{3+} in $LiGd_5P_2O_{13}$: Eu^{3+}, the decay lifetimes of Eu^{3+} were investigated. When there is no interaction between rare earth ions, the decay curve is usually a single exponential function. But the decay curves of LGPO: xEu^{3+} (x > 0.2) samples exhibit obvious deviations from the single exponential decay. Thus, the average decay time (τ) was determined by the following formula:

$$\tau = \frac{\int_0^\infty tI(t)dt}{\int_0^\infty I(t)dt} \quad (2)$$

As shown in Fig.4a and Tab.1, Decay time of $^5D_0$-$^7F_2$ transition decreases as Eu^{3+} contents increase. The $^5D_0$-$^7F_2$ decay time of LGPO: $0.1Eu^{3+}$ is 1260.46 μs, whereas that of LGPO: $1.0Eu^{3+}$ was 62.60 μs. The similar tendency happens in the Decay time of $^5D_0$-$^7F_4$ transition (Fig.4b),

which is a strong proof of enhanced non-radiative energy transfer between Eu^{3+} ions with shorten Eu^{3+}-Eu^{3+} distance. The decay time of the optimized-composition LGPO: $0.2Eu^{3+}$ phosphor seems to be quite long (> 1ms), which could cause phosphor quenching from high LED flux if encapsulating phosphors directly on LED chip. For the phosphors with long decay time, it is suggested that they are best used in remote phosphor package, in which a phosphor composite is precisely layered onto a substrate and separated from the LED energy source, in order to reduce the incident flux on the phosphor [17].

There are three type of electric multipolar interaction, i.e. dipole-dipole (d-d), dipole-quadrupole (d-q) and quadrupole-quadrupole (q-q) interactions. Thus, there is a need to elucidate which type of interaction is involved in energy transfer. According to Dexter's theory, the relation between luminescent intensity (I) and activator concentration (x) can be expressed by this equation [18]:

$$I / x = K[1 + \beta(x)^{Q/3}]^{-1} \quad (3)$$

where x is the activator concentration, I/x is the emission intensity (I) per activator concentration (x), and K and β are constants for the same excitation condition for a given host crystal. Q = 3 stands for energy transfer among the nearest neighbor ions, while Q = 6, 8 and 10 stands for dipole-dipole, dipole-quadrupole, and quadrupole-quadrupole interactions [19]. Eq.3 can thus be represented by the follow equation:

$$\tau / x = K[1 + \beta(x)^{Q/3}]^{-1} \quad (4)$$

As illustrated in Fig.5, the relationship of lg(τ/x) versus lg(x), using either $^5D_0$-$^7F_2$ or $^5D_0$-$^7F_4$ decay times, are linear. And the slope of the line is about -3. So the value of Q is approximately equal to 9, which clearly indicates that both dipole-quadrupole and quadrupole-quadrupole interactions play part in the concentration quenching process in LGPO: Eu^{3+}.

3.4 Judd-Ofelt parameters and radiative properties

The Judd-Ofelt (J-O) theory has been successfully applied to the quantitative determination of the optical properties of trivalent lanthanides [20]. The Judd-Ofelt intensity parameters ($\Omega_{2,4}$) provide valuable information about the local structure and bonding in the vicinity of rare earth ions. By analyzing the data from emission spectra and decay lifetimes, the local environment around the metal ion and the bond covalency of metal-ligand bonds can be interpreted [21].

As a representative sample, the data of $LiGd_5P_2O_{13}$: $0.2Eu^{3+}$ was analyzed by Judd-Ofelt theory. The total relative integrated intensity I ($I = \sum_{J=0-4} I_{^7F_J}$) is proportional to the total radiative transition rate $\sum_{J=0-4} A_{^7F_J}$, which is equal to the reciprocal of experimental lifetime τ. Therefore, the equation could be written as:

$$I = a \sum_{J=0-4} A_{^7F_J} = a \times \frac{1}{\tau} \quad (5)$$

where a is a constant. The branching ratio β corresponding to the emission from an excited level to

its lower levels is as follows:

$$\beta = \frac{A_{J'-J}}{\sum_{J=0-4} A_{J'-J}} \quad (6)$$

Thus, each $^5D_0$-^7F_J (J = 0, 1, 2, 3 and 4) radiative transition rate was calculated and shown in Tab.2.

The radiative transition rates of electric dipole transitions could be expressed as a function of the J-O intensity parameters [22]:

$$A^{ed}_{J'-J} = \frac{64\pi^4 v^3 e^2}{3h(2J'+1)} \frac{n(n^2+2)^2}{9} \sum_{J=2,4} \Omega_J \left\langle {}^5D_0 \left| U^{(J)} \right| {}^7D_J \right\rangle^2 \quad (7)$$

where n is the refractive index of host, h is Planck's constant (h = 6.626 × 10^{-27} erg s), v is the wave-number of radiative transition, and e is the charge of electron (e = 4.803 × 10^{-10} esu). The $\left\langle {}^5D_0 \left| U^{(J)} \right| {}^7D_J \right\rangle^2$ values are the square reduced matrix elements which are independent of the chemical environment of the Eu^{3+} ion.

The refractive index (n) could be calculated by following equation [23]:

$$A^{md}_{J'-J} = \frac{64\pi^4 v^3}{3h(2J'+1)} n^3 S_{md} \quad (8)$$

Where S_{md} is the magnetic dipole line strength (S_{md} = 7.83 × 10^{-42}). Therefore, a value of 2.01 for refractive index (n) could be obtained.

For $LiGd_5P_2O_{13}$: $0.2Eu^{3+}$, the value of Ω_2 and Ω_4 is found as 8.793 × 10^{-20} and 6.536 × 10^{-20} cm^2, respectively. It is known that Ω_2 is related to the covalency and structural changes in the vicinity of the Eu^{3+} ion (short range effect) while Ω_4 is not directly related to the symmetry of the Eu^{3+} ion but to the electron density on the surrounding ligands (long range effect) [24]. The great individual values of Ω_2 and Ω_4 indicate the great extent of the covalent character/electron density around the Eu^{3+} ion, and the high value of the ratio Ω_2/Ω_4 (>1) indicates the presence of Eu^{3+} in a highly asymmetric environment. The calculation results support the above-mentioned structural discussion and experimental observation of optical properties.

The stimulated emission cross-section (δ_e) was an essential parameter to signifies the rate of energy extraction from the lasing material and is calculated as [23]:

$$\sigma_e(\lambda_p) = [\frac{\lambda_p{}^4}{8\pi c n^2 \Delta\lambda_{eff}}] A_{J'-J} \quad (9)$$

where λ_P is the emission peak wavelength, c is the velocity of light and $\Delta\lambda_{eff}$ is the effective bandwidth of the emission transition. Effective bandwidth of the emission transition ($\Delta\lambda_{eff}$) and stimulated emission cross-section (δ_e) for each $^5D_0$-^7F_J transitions are shown in Tab.4. The product of emission cross-section and the effective bandwidth of the emission transition is a significant parameter to predictthe bandwidth of the optical amplifier. The higher the product

values were, the better was the amplifiers performance. $LiGd_5P_2O_{13}$: $0.2Eu^{3+}$ have comparable δ_e values of $^5D_0$-^7F_J transitions with those of reported BiOF:Eu^{3+}, indicating that it has some potential for red laser applications.

3.4 Temperature-dependent PL properties and quantum efficiency

The phosphor layers in LED devices are expected to operate at elevated temperatures (～150 °C) [25]. Therefore, the thermal quenching of LED phosphors is one of the most important technological parameters because it has great influence on the light output and CRI of devices. Thus, temperature-dependent PL spectra under 467 nm excitation of as-prepared $LiGd_5P_2O_{13}$: $0.2Eu^{3+}$ are indicated in Fig.6. The relative peak intensity (excitation at 467 nm and monitored at 622 nm) of LGPO: $0.2Eu^{3+}$ decreased marginally with rising temperature. It reached 80 % of initial value at 100 °C and then 70 % at 150 °C, which is better than reported $Sr_{1.7}Zn_{0.3}CeO_4$: Eu^{3+} (20 % at 150 °C) [26] and $Ba_2ZnB_2O_6$: Eu^{3+} (30 % at 150 °C) [27]. The fair thermal stability demonstrated that $LiGd_5P_2O_{13}$: Eu^{3+} red phosphor could be potential for high-powered LED applications. The internal quantum efficiency value (IQE) of LGPO: $0.20Eu^{3+}$ under 395 and 467 excitation is 46.5 %, which is comparable with previous reported $Sr_{1.7}Zn_{0.3}CeO_4$: Eu^{3+} (46.1 %) [26], and lower than commercialized red nitride phosphor $Sr_2Si_5N_8$: Eu^{2+} (78.2 %) [26]. However, the QE of LGPO: $0.20Eu^{3+}$ phosphor may be further boosted by optimizing the synthesis process.

4. Conclusions

In summary, the $LiGd_5P_2O_{13}$: Eu^{3+} phosphors were synthesized and systematically investigated. The phosphor could be excited efficiently by near-ultraviolet and blue light, and emits strong and high-purity red light. The CIE coordinate is calculated to be (0.644, 0.339). The optimum concentration of Eu^{3+} for $LiGd_{5(1-x)}P_2O_{13}$: xEu^{3+} is determined to be $x = 0.2$. By analyzing PL spectra and decay lifetimes, the critical distance (R_c) and the concentration quenching mechanism is found to be 13.86 Å and dipole/quadrupole-quadrupole interaction, respectively. From the Judd-Ofelt analysis, It is observed that the intensity parameter Ω_2 was greater than Ω_4. which suggest high covalency from the metal (Eu) to ligands (O), and the high value of the ratio Ω_2/Ω_4 (>1) indicates the presence of Eu^{3+} in a highly asymmetric environment. $LiGd_5P_2O_{13}$: Eu^{3+} exhibited efficient red emission (IQE = ~50 %) and good thermal stability (70 % at 150 °C). The results show that LGPO: Eu^{3+} may be considered as potential red emitting phosphor for NUV/blue pumped WLEDs.

Acknowledgement:

This research was supported by Guangxi Natural Science Foundation (Grant No. 2014GXNSFBA118046) and National Natural Science Foundation of China (No. 61264003).

References:

[1] Q. Zhou, Y. Zhou, Y. Liu, L. Luo, Z. Wang, J. Peng, J. Yan, M. Wu, *J. Mater. Chem. C*, 2015, 3, 3055.
[2] J. Zhou, F. Huang, J. Xu, H. Chen, Y. Wang, *J. Mater. Chem. C*, 2015, 3, 3023.
[3] N. Komuro, M. Mikami, Y. Shimomura, E.G. Bithell, A.K. Cheetham, *J. Mater. Chem. C*. 2015, 3, 204.
[4] Q. Liu, Z. Zheng, X. Zhang, Z. Bai, *J. Alloy. Compd.* 2015, 628, 298.
[5] H. Zhou, Y. Jin, M. Jiang, Q. Wang, X. Jiang, *Dalton Trans.* 2015, 44, 1102.
[6] X. Zhang, J. Zhang, M. Gong, *Opt. Mater.* 2014, 36, 850.
[7] X. Zhang, C. Zhou, J. Song, L. Zhou, M. Gong, *J. Alloy. Compd.* 2014, 592, 283.
[8] Y. Peng, W. Shi, C. Han, Y. Kang, Y. Wang, Z. Zhang, *Spectrochimica Acta, Part A,* 2015, 145, 194.
[9] F. Du. Y. Nakai, T. Tsuboi, Y. Huang, H. Seo, *J. Mater. Chem.* 2011, 21, 4669.
[10] G. Zhu, Z. Ci, Y. Shi, M. Que, Q. Wang, Y. Wang, *J. Mater. Chem. C*. 2013, 1, 5960.
[11] J. Zhu, W. Cheng, D. Wu. H. Zhang, Y. Gong, H. Tong, D. Zhao, *Inorg. Chem*. 2007, 46, 208.
[12] R.D. Shannon, *Acta Cryst.* 1976, A32, 751.
[13] X. Bai, G. Zhang, P. Fu, J. *Solid State Chem.* 2007, 180, 1792.
[14] X. Dong, J. Zhang, X. Zhang, Z. Hao, Y. Luo, *J. Alloy. Compd.* 2014, 587, 493.
[15] N. Zhang, C. Guo, H. Jing, *RSC Adv.* 2013, 3, 7495.
[16] X. Zhang, F. Mo, L. Zhou, M. Gong, *J. Alloy. Compd.* 2013, 575, 314.
[17] Y. Zhu, N. Narendran, *J. Light & Vis. Env.* 2008, 32, 115-119.
[18] D. Dexter, J. Schulman, *J. Chem. Phys.* 1954, 22, 1063.
[19] C. Huang, L. Luo, T. Chen, *J. Electrochem. Soc*. 2011, 158, J341.
[20] M.H.V. Werts, R.T.F. Jukes, J.W. Verhoeven, *Phys. Chem. Chem. Phys*. 2002, 4, 1542.
[21] C.R. Raju, C.A. Reddy, S. Sailaja, H. Seo, B.S. Reddy, *J. Mater. Sci.* 2012, 47, 772.
[22] R. Saraf, C. Shivakumara, S. Behera, N. Dhananjaya, H. Nagabuhushana, *RSC Adv.* 2015, 5, 9241.
[23] B. R. Judd, *Phys. Rev.* 1962, 127, 750-761.
[24] R. Shukla, S.K. Gupta, V. Grover, V. Nartarajah, A.K. Tyagi, *Dalton. Trans.* 2015, 44, 10628-10635.
[25] F. Kang, Y. Zhang, M. Peng, *Inorg. Chem*. 2015, 54, 1462-1473.
[26] H. Li, R. Zhao, Y. Jia, W. Sun, J. Fu, L. Jiang, S. Zhang, R. Pang, C. Li, *ACS Appl. Mater. Interfaces*. 2014, 6, 3163.
[27] H. Yi, F. Li, L. Wu, L. Wu, H. Wang, B. Wang, Y. Zhang, Y. Kong, J. Xu, *RSC Adv.* 2014, 4, 64244.

Figure captions:

Fig.1 XRD patterns of LGPO: xEu^{3+} (x = 0.2, 0.4, 0.6 and 0.8) phosphors (a), and the crystal structure of $LiGd_5P_2O_{13}$ with Gd polyhedra (b)

Fig.2 The PLE and PL spectra of LGPO: 0.2Eu^{3+} (a), and corresponding CIE chromaticity diagram with image under a 365 nm UV lamp (b)

Fig.3 Concentration dependence of PL spectra of LGPO: xEu^{3+} samples (λ_{ex} = 467 nm)

Fig.4 Decay curves of the Eu^{3+} fluorescence in LGPO: xEu^{3+} samples (excited at 467 nm, monitored at 622/706 nm)

Fig.5 the dependence of lg(τ/x) on lg(x) of LGPO: xEu^{3+} samples

Fig.6 Temperature-dependent PL spectra of LGPO: 0.2Eu^{3+} phosphor (λ_{ex} = 467 nm

Tab.1 The average decay lifetimes of $^5D_0$-$^7F_{2,4}$ transition in LGPO: xEu^{3+} samples

Compounds	**$^5D_0$-$^7F_2$ decay lifetime (μs)**	**$^5D_0$-$^7F_4$ decay lifetime (μs)**
LGPO: 0.1Eu^{3+}	1260.46	1210.08
LGPO: 0.2Eu^{3+}	885.53	879.57
LGPO: 0.3Eu^{3+}	579.87	574.05
LGPO: 0.4Eu^{3+}	379.57	351.85
LGPO: 0.5Eu^{3+}	260.23	249.02
LGPO: 0.6Eu^{3+}	105.23	101.40
LGPO: 0.7Eu^{3+}	100.74	95.96
LGPO: 0.8Eu^{3+}	62.60	58.63
LGPO: 1.0Eu^{3+}	46.72	42.94

Tab.2 Judd-Ofelt parameters (transition rates, branching ratios, Ω_2 and Ω_4), effective bandwidth of the emission transition ($\Delta\lambda_{eff}$), stimulated emission cross-section (δ_e) in $LiGd_5P_2O_{13}$: 0.2Eu^{3+}

$LiGd_5P_2O_{13}$: 0.2Eu^{3+}						
Transition	**Wavenumber (cm^{-1})**	**Transition rate (s^{-1})**	**β (%)**	**Ω_J ($\times 10^{-20}$ cm^2)**	**$\Delta\lambda_{eff}$ (nm)**	**δ_e ($\times 10^{-22}$ cm^2)**
$^5D_0$-$^7F_0$	17256.25	31.964	2.83		3.25	3.640
$^5D_0$-$^7F_1$	16849.19	95.496	8.45		8.00	4.861
$^5D_0$-$^7F_2$	16090.10	691.00	61.15	8.793	18.5	18.29
$^5D_0$-$^7F_3$	15313.93	35.566	3.15		7.95	2.652
$^5D_0$-$^7F_4$	14164.30	251.84	22.29	6.536	7.25	28.33

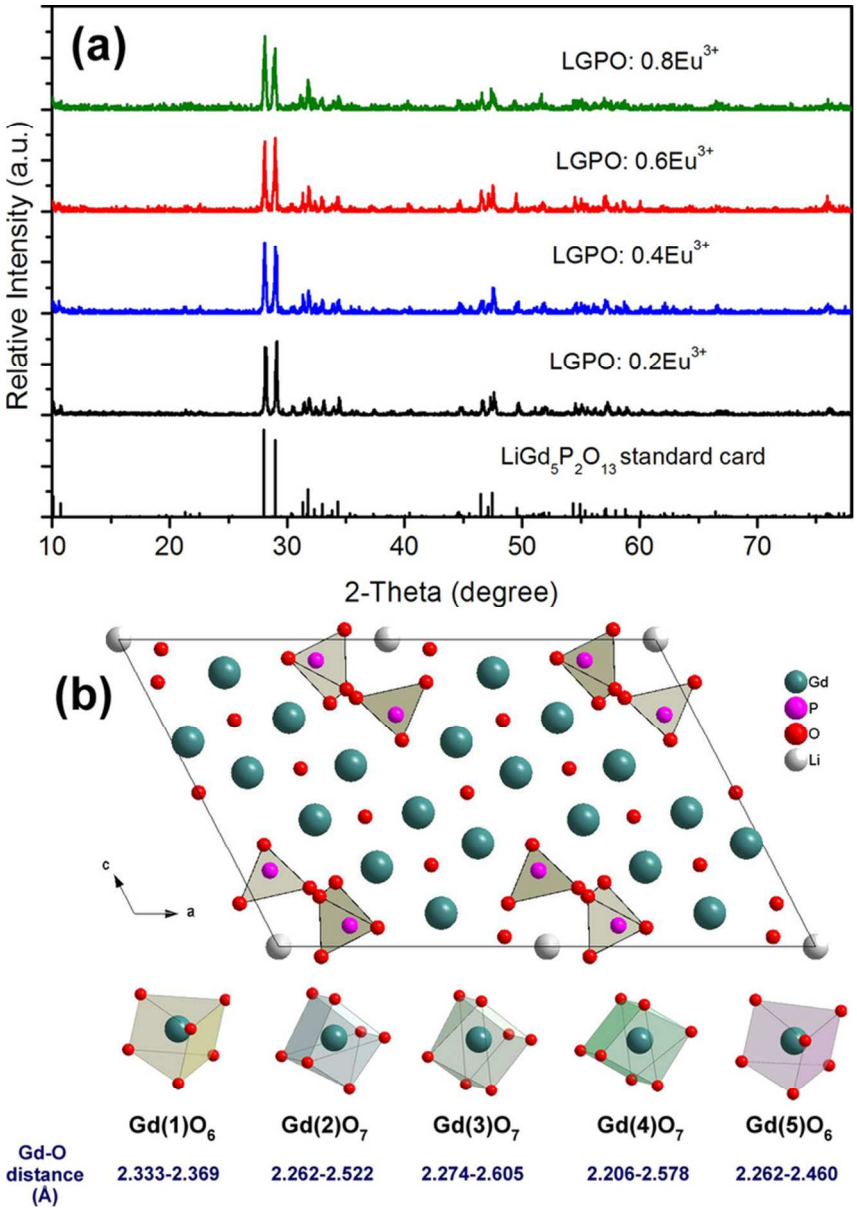

Fig.1 XRD patterns of LGPO: xEu3+ (x = 0.2, 0.4, 0.6 and 0.8) phosphors (a), and the crystal structure of LiGd5P2O13 with Gd polyhedra (b)
65x93mm (300 x 300 DPI)

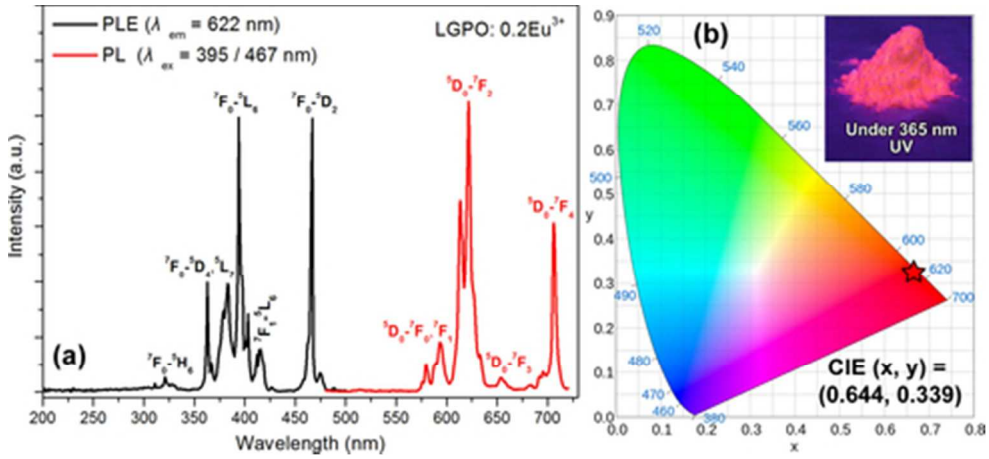

Fig.2 The PLE and PL spectra of LGPO: 0.2Eu3+ (a), and corresponding CIE chromaticity diagram with image under a 365 nm UV lamp (b)
41x18mm (300 x 300 DPI)

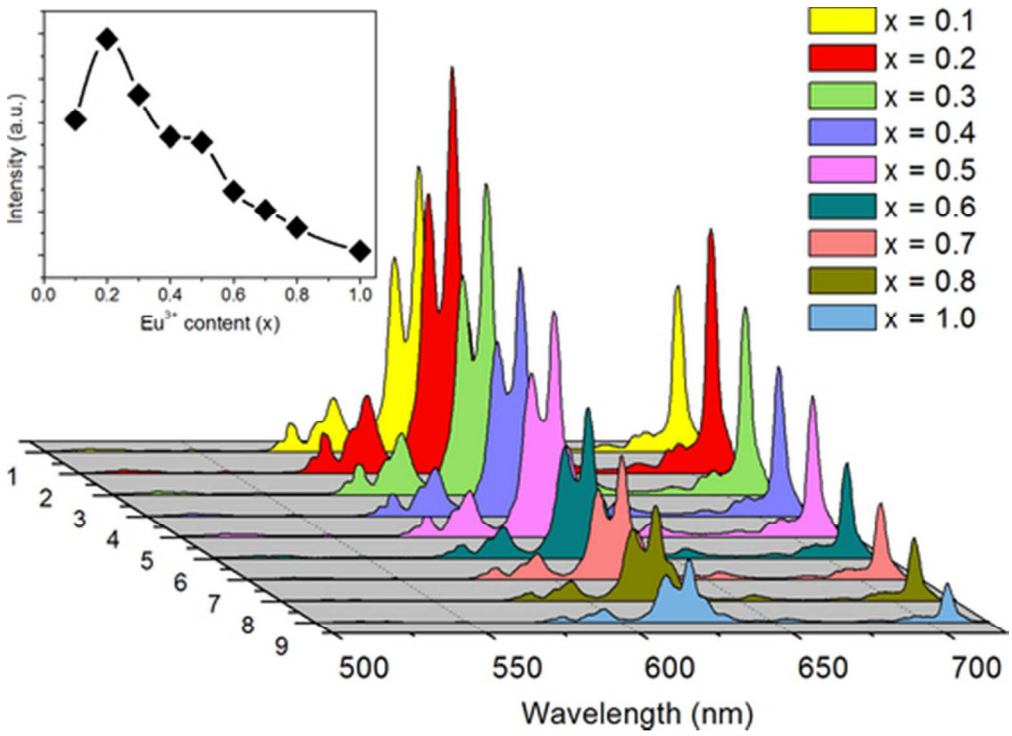

Fig.3 Concentration dependence of PL spectra of LGPO: xEu3+ samples (λex = 467 nm)
42x30mm (300 x 300 DPI)

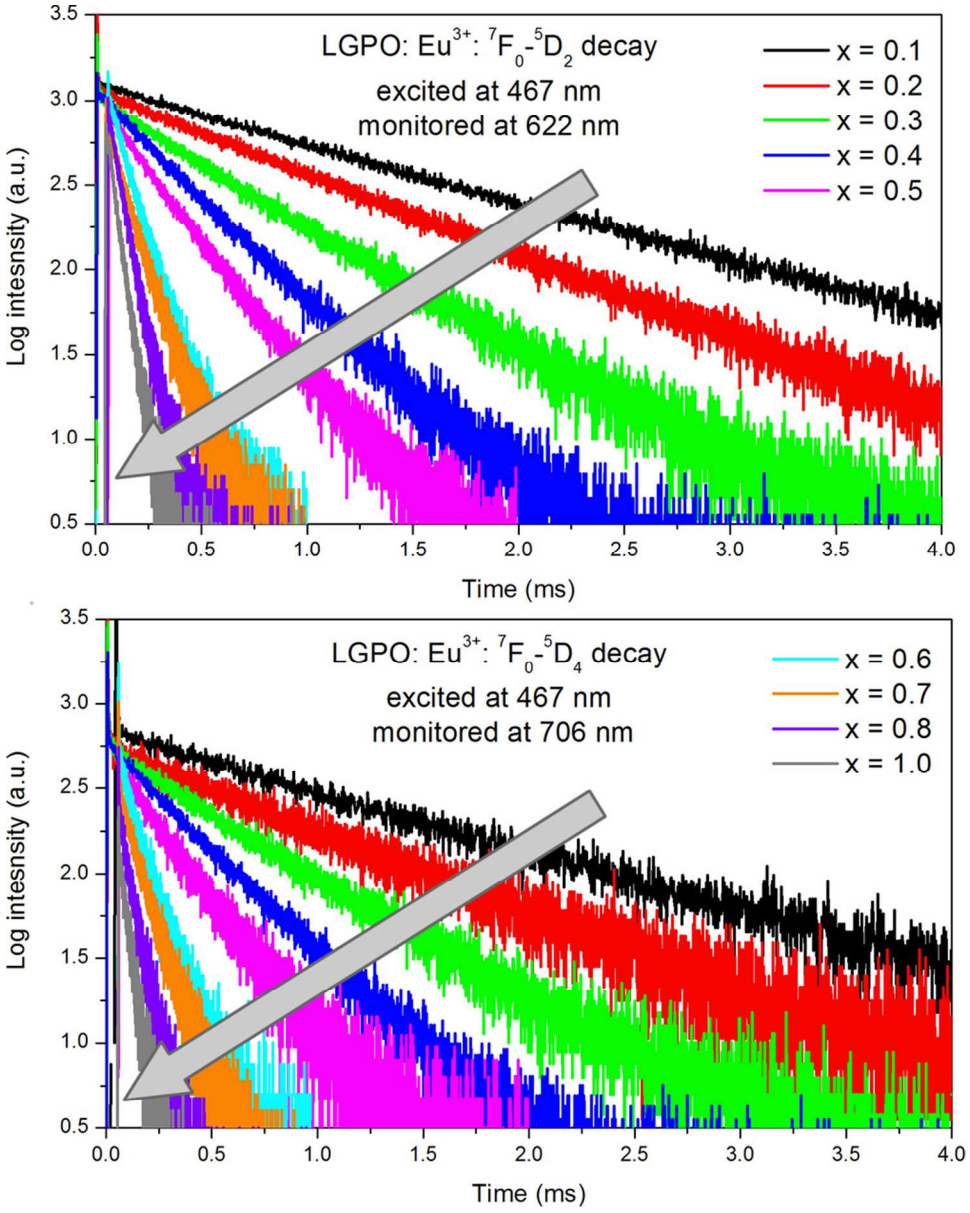

Fig.4 Decay curves of the Eu3+ fluorescence in LGPO: xEu3+ samples (excited at 467 nm, monitored at 622/706 nm
85x106mm (300 x 300 DPI)

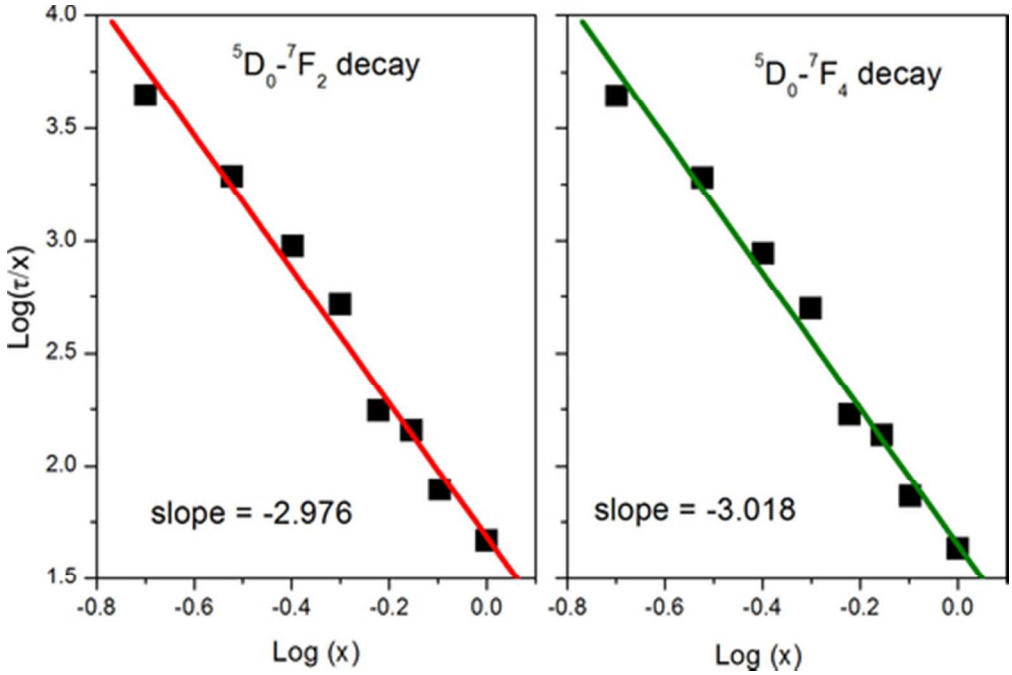

Fig.5 the dependence of lg(τ/x) on lg(x) of LGPO: xEu3+ samples
42x28mm (300 x 300 DPI)

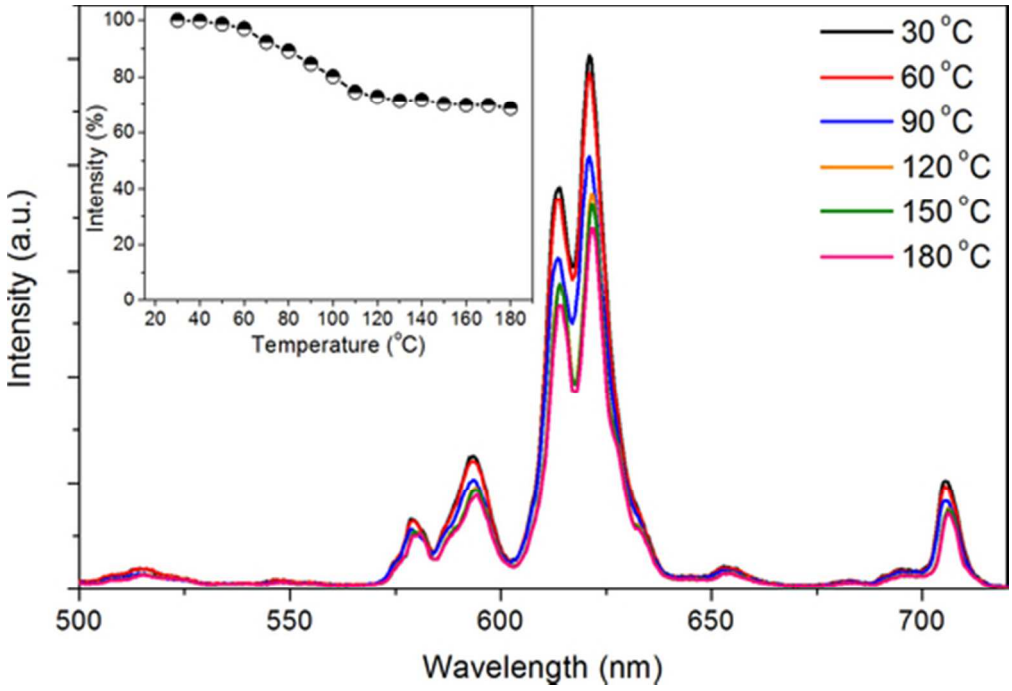

Fig.6 Temperature-dependent PL spectra of LGPO: 0.2Eu3+ phosphor (λex = 467 nm)
43x29mm (300 x 300 DPI)